Energies and hyperfine splittings of the 7*D* levels of atomic francium

J. M. Grossman,* R. P. Fliller III, T. E. Mehlstäubler,† L. A. Orozco, M. R. Pearson, G. D. Sprouse, and W. Z. Zhao‡
Department of Physics and Astronomy, State University of New York, Stony Brook, New York 11794-3800
(Received 5 May 2000; published 12 October 2000)

We report optical double-resonance spectroscopy to locate and study the $7D_{3/2}$ and $7D_{5/2}$ levels of a sample of ^{210}Fr atoms confined and cooled in a magneto-optical trap. The upper state of the $7P_{3/2}$ trapping transition serves as the resonant intermediate level to reach the $7D$ states. The energy difference to the ground state is measured for the accessible levels. We measure the hyperfine splittings: $\Delta(7D_{3/2},F=15/2\leftrightarrow 13/2)=167\pm 4$ MHz, $\Delta(7D_{5/2},F=17/2\leftrightarrow 15/2)=-117.5\pm 2.5$ MHz, and $\Delta(7D_{5/2},F=15/2\leftrightarrow 13/2)=-121\pm 4$ MHz. Extrapolating the energies of the inaccessible hyperfine levels from the hyperfine constants and assuming $B(7D_{3/2})=0$, the center-of-gravity energy difference to the ground state is $E(7D_{3/2})=24\,244.831\pm 0.003$ cm^{-1} and $E(7D_{5/2})=24\,333.298\pm 0.003$ cm^{-1}.

PACS number(s): 32.30.−r, 32.10.Fn, 32.80.Pj, 32.70.Jz

I. INTRODUCTION

The theoretical and experimental understanding of the low-lying *S* and *P* electronic states of francium is beginning to reach a level comparable to that of the other alkali-metal atoms [1–4]. Their energies, dipole matrix elements and hyperfine constants show that the heaviest alkali, even though it is radioactive, is subject to quantitative analysis that makes it a very promising candidate for precision measurement tests of fundamental symmetries in nature [5]. To further increase our understanding of this atom, the low-lying *D* states have to enter the picture. The very different angular momentum properties of these states add some additional complications to the quantitative understanding of the simplest of the heavy elements.

Optical double resonance is a well-established tool of laser spectroscopy [6]. It allows the study of an excited state through an intermediate, well-characterized one. The development of laser trapping and cooling techniques opened further its applicability. The magneto-optical trap (MOT) [7] operates in a regime where some population is in the upper state, making it an ideal intermediate state for optical double-resonance studies [8–11].

Francium is a short-lived radioactive alkali that we are able to study now thanks to laser trapping and cooling techniques [12]. The number of atoms captured in a MOT and cooled to a fraction of a mK is enough for optical double-resonance spectroscopy. In this paper, we present the location of the second excited state in the *D* series, the $7D$ state of ^{210}Fr, and a measurement of its hyperfine splitting. To find the state, we use a semi-empirical approach based on an extrapolation of a quantum defect fit (QDF) of the previously measured high-lying states of the nD series [13].

Since the trapping laser is intense, the upper state of the cycling transition has a significant ac Stark splitting (Autler-Townes). We resolve this line splitting intrinsic to the cooling process and study in a simplified model its influence on the precision of our measurements. We have to rely on such models to study many of the possible systematic effects present in the optical double resonance in a MOT since we do not have the possibility to study them directly, given the availability of Fr.

The following section of the paper describes the trapping of Fr and experimental techniques of exciting and detecting the $7D$ states. Section III relates *ab initio* and semi-empirical calculations of the energies of the $7D$ states; it also describes numerical modeling of the Autler-Townes splitting of the transition. Section IV describes the measurements of the hyperfine structure of the $7D$ states and studies of the different contributions to the measurement uncertainty. We report the results of the measurements of the hyperfine splittings, the energies, and the fine structure in Sec. V. The conclusions are presented in Sec. VI. The Appendix describes how the detuning frequency of the trap laser may be obtained from the observed Autler-Townes splittings.

II. TRAPPING FR AND EXCITATION OF THE 7*D* LEVELS

A. MOT and probe operation

The operation of the magneto-optical trap (MOT) for Fr has been described previously [14]. Briefly, to make ^{210}Fr, a 100-MeV beam of ^{18}O ions from the Stony Brook superconducting linear accelerator impinges on a gold target. We extract $\approx 1\times 10^6$ francium ions/s out of the gold and transport them about 1 m to a hot yttrium neutralizer. From here, the neutral atoms enter a dry-film coated glass cell where they are cooled and trapped in the MOT with 10^3–10^4 atoms captured in steady state. Each of the six intersecting MOT beams has a $1/e^2$ (power) diameter of 4 cm and a typical power of 50 mW. The field gradient is 6 G/cm. The trap operates on-line in the target room of the accelerator, and we remotely control the experiment.

Figure 1 shows the energy levels of ^{210}Fr relevant for trapping and spectroscopy. A Coherent 899-21 titanium-sapphire laser operating at 718 nm excites the trapping and cooling transition $7S_{1/2}$, $F=13/2\rightarrow 7P_{3/2}$, $F=15/2$ (τ

*Electronic address: Joshua.Grossman@sunysb.edu
†Present address: Institut für Quantenoptik der Universität Hannover, D-30167 Hannover, Germany.
‡Present address: RSM Electron Power, Inc., Deer Park, NY 11729.

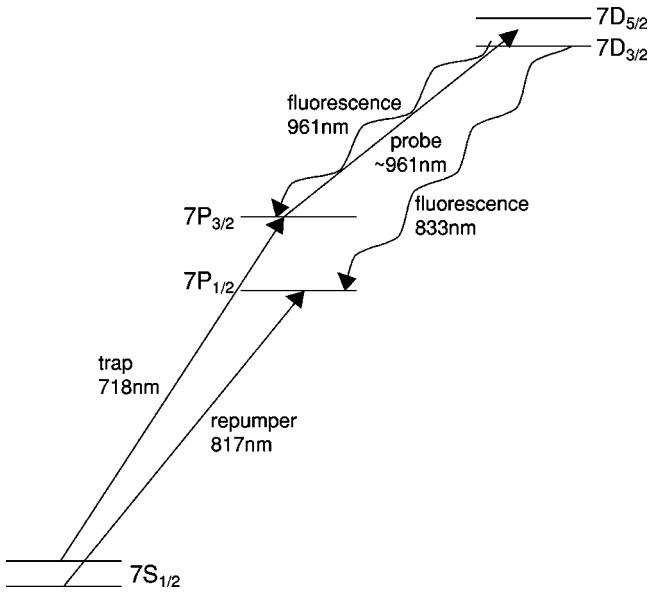

FIG. 1. Energy levels and transitions in ^{210}Fr. Only the ground-state hyperfine splitting is shown.

$=21$ ns [15]). An EOSI 2010 diode laser at 817 nm repumps any atoms that leak out of the cooling cycle via the $7S_{1/2}$, $F=11/2 \rightarrow 7P_{1/2}$, $F=13/2$ transition. The lack of an absolute frequency reference to the atomic resonances of Fr prevents us from knowing the laser detunings for operating the trap. We present in the Appendix an indirect measurement of the trap laser detuning. A computer-controlled scanning Fabry-Perot cavity monitors and holds the long-term frequencies of both the trap laser and the repumper [16]. A charge-coupled-device camera monitors the trap fluorescence.

We use two-photon excitation to probe the $7D$ levels. The resonant intermediate level is the upper state of the trapping transition $7P_{3/2}$, $F=15/2$. A second Coherent 899-21 titanium-sapphire laser operating at 969 nm or 961 nm excites the transition from the intermediate level to the $7D_{3/2}$ or $7D_{5/2}$ levels, respectively. Only the upper two hyperfine levels ($F=13/2,15/2$) of the $7D_{3/2}$ state and the $F=13/2,15/2$, and 17/2 levels of the $7D_{5/2}$ state are accessible from the intermediate level.

Figure 2 shows a block diagram of the experiment. A Burleigh WA-1500 wavemeter measures the frequencies of all three lasers. We calibrate this instrument in absolute terms against known transitions in Rb [17]. We correct for any deviation of the readings from the Rb transition frequencies, even though the largest deviation (2×10^{-3} cm^{-1}) was within the precision (2×10^{-3} cm^{-1}) of the wavemeter. In contrast to some of our previous work (for example, [18]), we do not have access to calibrated lines in the iodine spectrum near 960 nm to which to calibrate the wavemeter.

B. Methods of detection

There are several constraints in our particular experiment that require careful attention to optimize the signal-to-noise ratio for our results. Our detection channel is always fluorescence. In some cases it is at a different wavelength from that

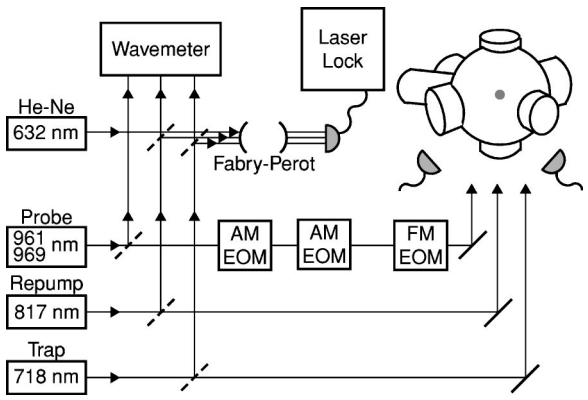

FIG. 2. Block diagram of experiment.

of the excitation, in which case we discriminate it from the excitation with an interference filter. In other cases, because it is at the same wavelength, we cannot discriminate it from the excitation by color, so we do so by timing.

When we have a well-differentiated wavelength to detect, we perform continuous wave excitation and look for resonances using photon counting techniques. This is the case for the study of the $7D_{3/2}$ state that can emit a $7D_{3/2} \rightarrow 7P_{1/2}$ fluorescence photon at 833 nm that is detected and discriminated (see Fig. 1 for the relevant energy levels). Our main source of background is scattered light from the MOT lasers, so we reduce the aperture of the detector optical system to decrease it. At this wavelength and with the narrow-band interference filter (2 nm), the contribution from the blackbody radiation emitted by the yttrium neutralizer at 1000 K is negligible. The interference filter also blocks the 817-nm light scattered off the glass cell. A Hamamatsu R636-10 photomultiplier tube (PMT) operating in photon counting mode detects the 833-nm fluorescence of the decay.

Because the $7D_{5/2}$ level does not decay to the $7P_{1/2}$ level, we use a different detection technique. Two cascaded Gsänger LM0202 electro-optic modulators (EOMs) extinguish the excitation laser, and we look for the fluorescence in a time window after the extinction of the light. A Hamamatsu R2658P PMT operating in photon counting mode with appropriate interference filters detects the 961-nm fluorescence of the decay from the $7D_{5/2} \rightarrow 7P_{3/2}$ level. However, the quantum efficiency of this PMT ($\approx$0.3% at 961 nm) is more than an order of magnitude worse than that of the R636-10 ($\approx$7% at 833 nm). At this wavelength, scattered blackbody radiation from sources such as the nearby hot neutralizer cannot be completely excluded.

Another method of detection of an atomic resonance is the fluorescence decrease of the trapping transition whenever some atoms absorb other radiation [8]. We have used this reduction in the signal for the initial detection of the $7D_{5/2}$ level, but it has a poor signal-to-noise ratio.

III. THEORY

A. Quantum-defect fit (QDF)

The *ab initio* many-body perturbation calculations by Dzuba *et al.* [3] of the ionization energy of the $7D_{3/2}$ and

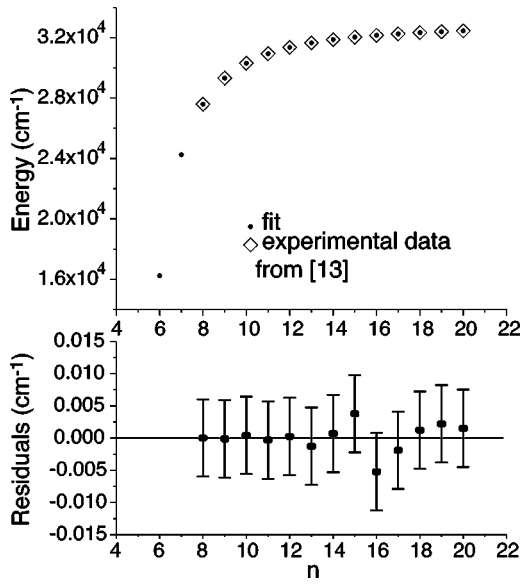

FIG. 3. Quantum-defect fit to the $nD_{3/2}$ series using experimental data from Ref. [13].

$7D_{5/2}$ states have an expected uncertainty of a few tenths of a percent. A search of even 0.1% or 16 cm^{-1} would be difficult, so we use a quantum-defect fit to the other measured D states as a guide. Previous experiments in Fr [18,19] show that QDF gives predictions accurate to better than 1 cm^{-1}. The energies of the series of nD_J ($J=3/2,5/2$) levels of francium can be represented by the Rydberg series

$$E(nD_J)=E_{\rm ion}-\frac{R_{\rm M}}{n_{\rm eff}^2}, \tag{1}$$

where $E_{\rm ion}$ is the ionization energy of the ground state, $E(nD_J)$ is the energy of the nD_J level measured from the ground state, and $R_{\rm M}$ is the reduced mass Rydberg constant. Equation (1) assigns an effective quantum number $n_{\rm eff}$, to the known francium nD_J levels. We use an iterative algorithm to fit the quantum-defect parameters δ_0, δ_2 δ_4, and δ_6 to the previously measured energies in the series using

$$n_{\rm eff}=n-\delta$$
$$=n-\left(\delta_0+\frac{\delta_2}{(n-\delta)^2}+\frac{\delta_4}{(n-\delta)^4}+\frac{\delta_6}{(n-\delta)^6}+\cdots\right), \tag{2}$$

where δ is the quantum defect. We use the energies of the nD_J ($n=8,\ldots,20$) states previously measured in ^{212}Fr by Arnold *et al.* [13] to predict the location of the $7D_J$ states in ^{210}Fr, taking into account the isotope shift of the ground state [20]. Since the density of d electrons at the nucleus is negligible, we neglect the isotope shift of the D states. Figure 3 shows the quantum-defect fit for the $nD_{3/2}$ series. Furthermore, once the energy of one of the 7D states has been measured, a second prediction for the remaining level can be obtained from the empirical formula for the fine-structure splittings $\Delta E_{\rm fine}(n)$ of series states

$$\Delta E_{\rm fine}(n)=an_{\rm eff}^{-3}+bn_{\rm eff}^{-5}, \tag{3}$$

where a and b are constants. $n_{\rm eff}$ is given in Eq. (1), but it is calculated using the center of gravity of the nD series instead of a specific nD_J series. This formula has been shown to hold in earlier studies on Rydberg series in He, Na, and Rb [21].

B. The Autler-Townes effect

In an idealized three-level atom, in the limit of a strong trap laser and a weak probe laser, the probe transition is split and shifted by [22]

$$\frac{\Delta E_{\rm AT}}{\hbar}=-\frac{\delta_{\rm trap}}{2}\pm\frac{\sqrt{\delta_{\rm trap}^2+\Omega_{\rm trap}^2}}{2}, \tag{4}$$

where $\delta_{\rm trap}$ and $\Omega_{\rm trap}$ are the trap laser detuning and Rabi frequency, respectively. To lowest order, as given by Eq. (4), the average of the peak centers of the two peaks of an Autler-Townes doublet should give the unsplit line center shifted by $\delta_{\rm trap}$. To obtain an estimate of higher-order effects than those described by Eq. (4), we perform numerical calculations using (four+two)-level optical Bloch equations, following the treatments given in Refs. [23,24]. This model suffices to give a qualitative picture of the Autler-Townes effect in two-photon transitions to different hyperfine levels. For a quantitative comparison with the data, we would need a more complete description that includes each hyperfine level's $2F+1$ magnetic sublevels and their statistical weights. As the atoms occupy a volume of ≈ 1 mm^3, these sublevels are in turn perturbed by the inhomogeneous (6-G/cm gradient) magnetic field of the MOT and by the spatially varying intensity and polarization of the light field.

In the optical Bloch equation calculations, the four main levels are the upper ground state ($7S_{1/2}$, $F=13/2$), the intermediate state ($7P_{3/2}$, $F=15/2$), and the two accessible hyperfine states of the $7D_{3/2}$ level ($7D_{3/2}$, $F=13/2$ and $F=15/2$). We also include two additional levels to account for decays via the $7P_{1/2}$ levels and for off-resonant excitation to the wrong hyperfine level of the $7P_{3/2}$ state and subsequent decay to the lower ground state. The optical Bloch equations describe the evolution of the density matrix ρ that gives the atomic level populations and coherences in the laser field. The equations may be simplified by introducing the slowly varying quantity σ_{nm} such that

$$\rho_{nm}(t)=\sigma_{nm}(t)\exp(-i\omega_{nm}^0 t), \tag{5}$$

where $\omega_{nm}^0=(E_n-E_m)/\hbar$ is the transition angular frequency and n and m refer to the levels involved in the transition. In the steady state, the optical Bloch equations are then

$$\sum_k(\gamma_{kn}\sigma_{kk}-\gamma_{nk}\sigma_{nn})+\frac{i}{2}\sum_k(\Omega_{nk}\sigma_{kn}-\sigma_{nk}\Omega_{kn})$$
$$=0 \quad \text{for } n=m,$$

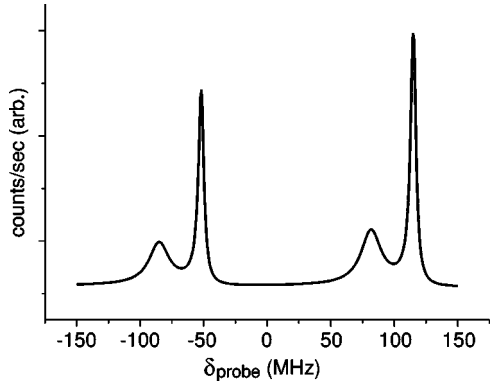

FIG. 4. Numerical solution of the four-level optical Bloch equations that model the fluorescence from the upper two hyperfine levels of the $7D_{3/2}$ level as a function of probe laser detuning. The reference for the detuning is a frequency halfway between the two unshifted transitions to accessible $7D_{3/2}$ hyperfine states. $\tau(7P_{3/2}) = 21$ ns, $\tau(7D_{3/2}) = 73.6$ ns, $\delta_{\mathrm{trap}}(7S_{1/2}\rightarrow 7P_{3/2})/(2\pi) = -31.7$ MHz, $\Omega_{\mathrm{trap}}(7S_{1/2}\rightarrow 7P_{3/2})/(2\pi) = 15$ MHz, $\Omega_{\mathrm{probe}}(7P_{3/2}\rightarrow 7D_{3/2}, F=13/2)/(2\pi)=7/8$ MHz, and $\Omega_{\mathrm{probe}}(7P_{3/2}\rightarrow 7D_{3/2}, F=15/2)/(2\pi) = 1$ MHz.

$$(i\delta_{nm}-\Gamma_{nm})\sigma_{nm}+\frac{i}{2}\sum_k(\Omega_{nk}\sigma_{km}-\sigma_{nk}\Omega_{km}) = 0 \quad \text{for } n\neq m, \tag{6}$$

where δ_{nm} and Ω_{nm} are the laser detuning and Rabi frequency for the transition from level n to m, and γ_{nm} is the radiative decay rate from level n to m. The damping rate of off-diagonal terms is

$$\Gamma_{nm}=\frac{1}{2}\sum_k(\gamma_{nk}+\gamma_{mk}). \tag{7}$$

We neglect dephasing due to processes such as collisions. Equations 6 describe a 36×36 matrix for our $(4+2)$-level system. Figure 4 shows a spectrum calculated this way for parameters similar to those of the experiment (see the Appendix). The ratio of the Rabi frequencies of the transitions to the two $7D$ hyperfine levels is the ratio of their statistical weights, as given by the number of sublevels and as observed in the relative resonance peak amplitudes in the measured fluorescence.

In our calculations, the Autler-Townes splitting decreases with increasing probe power. In the weak probe regime, however, the effect is too small (<100 kHz) to be resolved in our experiment. As a function of probe power, our calculations also show a small shift in the line center of each split transition as obtained from a fit of the Autler-Townes doublet line shape. This shift arises because the $7P_{3/2}\leftrightarrow 7D_J$ excitation and decay cycle is not closed. For detunings at which more atoms are excited from the $7P_{3/2}$ to the $7D_J$ level, atoms are depleted from the trapping cycle and join the upper cycle. Additionally, excitation to the $7D_J$ and subsequent decay may optically pump atoms to the lower ground state [8]. The change in the population available to make the $7P_{3/2}\leftrightarrow 7D_J$ transition as the laser scans across resonance causes an apparent shift in the line center. Because this shift is different for each hyperfine level, it affects measurements of the hyperfine splittings. Like the dependence of the splitting on the probe power, the shift of the line center is too small in the weak probe regime to be resolved in this experiment (see Fig. 5). Even though our calculations show that these effects are small, we do search for any systematic effect they may have on our measurements, as described in Sec. IV B.

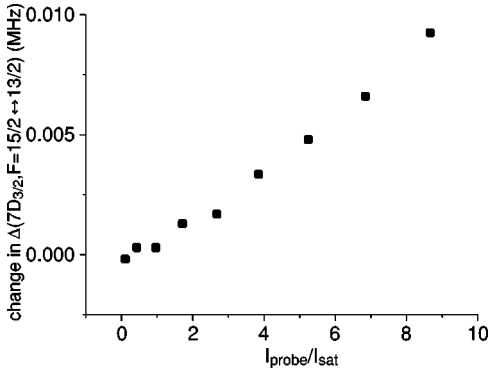

FIG. 5. Numerical optical Bloch equation calculation of the shift in the apparent value of the hyperfine splitting $\Delta(7D_{3/2}, F=15/2\leftrightarrow 13/2)$ using line centers obtained by averaging fitted centers of Autler-Townes peaks.

IV. MEASUREMENT OF THE HYPERFINE STRUCTURE

A. Hyperfine splittings

The experimental measurements of the location of the energy levels and their hyperfine splittings are simultaneous. Our sample of atoms is very cold (less than a few hundred μK) with negligible Doppler broadening, so although the hyperfine splittings are of the order of 100 MHz they are resolvable. To increase our frequency resolution, a New Focus 4002 EOM applies 60-MHz or 100-MHz radio-frequency (RF) sidebands to the probe laser, with the applied

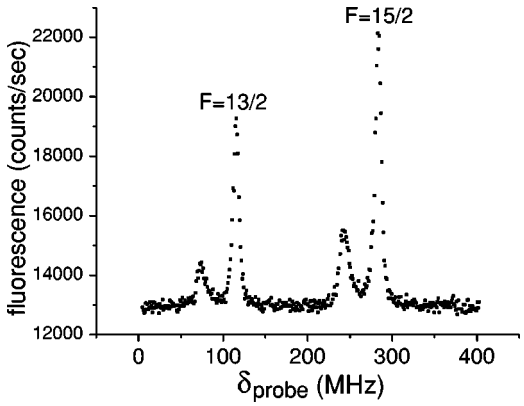

FIG. 6. Scan of the $7D_{3/2}$ state (without RF sidebands). The $F=13/2$ and $F=15/2$ hyperfine levels are indicated. The transition to each hyperfine level is further split by the Autler-Townes effect due to the strong trap laser.

TABLE I. Error budget for measurements of the hyperfine splittings (HFS).

HFS (MHz)	$\Delta(7D_{3/2}, F=15/2\leftrightarrow 13/2)$ 167		$\Delta(7D_{5/2}, F=17/2\leftrightarrow 15/2)$ 117.5		$\Delta(7D_{5/2}, F=15/2\leftrightarrow 13/2)$ 121	
Error	(MHz)	%	(MHz)	%	(MHz)	%
Statistical	3.9	2.34%	2.3	2.0%	4.1	3.4%
Peak center fitting	0.01	<0.01%	0.5	0.4%	1.0	0.8%
Zeeman	0.6	0.36%	0.7	0.6%	0.8	0.7%
$P_{\text{probe}}, P_{\text{trap}}, \delta_{\text{trap}}$	<0.01	<0.01%				
correlation with A-T	<0.01	<0.01%				
trap depletion	<0.01	<0.01%				
Total	**4.0**	**2.4%**	**2.5**	**2.1%**	**4.3**	**3.4%**

frequency stable to better than 1 part in 10^6. The RF sidebands serve as an *in situ* calibrated meter for the frequency scale of the laser scan.

Figure 6 shows a scan of the $7D_{3/2}$ level. The hyperfine levels are indicated on the scan. Only two hyperfine levels of the $7D_{3/2}$ state and three levels of the $7D_{5/2}$ state are accessible. We identify the components of the spectrum by comparing their relative intensities with the transition line strengths. The hyperfine structure of the $7D_{5/2}$ state is inverted, as is typical of the $D_{5/2}$ states of the other alkalis ([9,10], for example). The transition to each hyperfine level is further split by the Autler-Townes effect due to the presence of the strong trap laser.

The shift of a hyperfine level of total angular momentum quantum number F is given by

$$\frac{\Delta E_{\text{hf}}}{\hbar} = A\frac{K}{2} + B\frac{3K(K+1) - 4I(I+1)J(J+1)}{8I(2I-1)J(2J-1)}, \quad (8)$$

where $K = F(F+1) - I(I+1) - J(J+1)$ with I as the nuclear spin.

For scans of the $7D_{5/2}$ state, we take the line center to be the average of the Autler-Townes peak centers, as discussed in the previous section. The signal-to-noise ratio of these scans is such that this approximation suffices. For scans of the $7D_{3/2}$ hyperfine structure, several systematics were tested to measure deviations from this simple model. For these measurements, the probe laser was attenuated to intensities <4 mW/cm^2 with most measurements using ≈ 0.5 mW/cm^2. For an ideal two-level atom, the saturation intensity for this transition is $I_{\text{sat}}(7P_{3/2} \rightarrow 7D_{3/2}) = 3.1$ mW/cm^2. Including the magnetic sublevels of the upper and lower state increases I_{sat}, as demonstrated by Dineen *et al.* [25].

B. Systematic studies

The main limitations on the signal to noise of the laser scans were the quantum efficiency of the PMTs and background light from the hot neutralizer and the other lasers. These effects were greatest for the $7D_{5/2}$ level scans. Refer to Table I for the error budget for the measurements of the hyperfine splittings. The RF sidebands allow us to check that there is no measurable nonlinearity to the probe laser scans.

As discussed in Sec. IV A, while the probe-laser scans through resonance atoms may be depleted from the trapping cycle and enter the probe cycle. Some of these atoms stay in the trap volume, while others leave the trap volume and, consequently, the probe interaction region. Both of these changes in the population of atoms interacting with the probe laser as its frequency scans can shift the apparent line center of the probed transition. To avoid this, a weak probe is used and the trapping cycle fluorescence is monitored so that it does not decrease by more than 20%. We also make an equal number of scans with increasing frequency and decreasing frequency to average out possible asymmetries due to trap depletion. We check that no correlations of the Autler-Townes splitting with probe power are found, indicating that the weak probe and strong trap laser limit is appropriate. Furthermore, no correlations are found between the measured hyperfine splitting and the probe power, the trap laser power, the trap laser detuning, the Autler-Townes splitting, or the direction of the probe scan.

TABLE II. Comparison of measured and predicted hyperfine constants. Structural radiation contributions have not been included in the calculations of Ref. [26]. For the D states these contributions are not small.

Source	$A(7D_{3/2})$ (MHz)	$A(7D_{5/2})$ (MHz)	$B(7D_{5/2})$ (MHz)
This work	**22.3(5)** [a]	**−17.8(8)**	**64(17)**
Ref. [26] (MBPT)	11.3(3)	-19.5(5)	
Ref. [27] (MBPT)	24.8	-12.8	

[a]Assuming $B(7D_{3/2}) = 0$.

TABLE III. Energy from accessible hyperfine levels to the ground-state center of gravity.

State	E (cm^{-1})
$7D_{3/2}, F=15/2$	24 244.838(4)
$7D_{3/2}, F=13/2$	24 244.832(4)
$7D_{5/2}, F=17/2$	24 333.291(4)
$7D_{5/2}, F=15/2$	24 333.294(4)
$7D_{5/2}, F=13/2$	24 333.298(4)

An imbalance of the trapping beams can push the trapped atoms to a point of nonzero magnetic field. Optical pumping to an average population occupation of a magnetic sublevel $m_F \neq 0$ can cause a shift of a resonance that depends on F. We place an upper limit on this shift by considering a displacement of one trap diameter and complete population occupation of the magnetic sublevels that cause the greatest change in the hyperfine splitting (yet can be reached from a common intermediate state). In this case, the $\Delta(7D_{3/2},\ F=15/2 \leftrightarrow 13/2)$ splitting is shifted by 0.6 MHz, $\Delta(7D_{5/2},\ F=17/2 \leftrightarrow 15/2)$ by 0.7 MHz, and $\Delta(7D_{5/2},\ F=15/2 \leftrightarrow 13/2)$ by 0.8 MHz. The observed symmetry of the transition line shapes indicates that neither a pathological Zeeman shift nor depletion of the trap seem to contribute significantly to the measured line centers.

V. RESULTS

A. Hyperfine splittings

The predominant error is statistical with a small contribution from fitting error and systematics. The final measured values of the hyperfine splitting are $\Delta(7D_{3/2},\ F=15/2 \leftrightarrow 13/2) = 167 \pm 4$ MHz, $\Delta(7D_{5/2},\ F=17/2 \leftrightarrow 15/2) = -117.5 \pm 2.5$ MHz, and $\Delta(7D_{5/2},\ F=15/2 \leftrightarrow 13/2) = -121 \pm 4$ MHz. Since only the upper two hyperfine levels of the $7D_{3/2}$ state are accessible, only one hyperfine interaction constant can be obtained. We assume no quadrupole term in Eq. (8): $B(7D_{3/2})=0$. With this assumption, the hyperfine constants are $A(7D_{3/2}) = 22.3 \pm 0.5$ MHz, $A(7D_{5/2}) = -17.0 \pm 0.8$ MHz, and $B(7D_{5/2}) = 64 \pm 17$ MHz. Altering $A(7D_{3/2})$ by one standard deviation (0.5 MHz) requires $B(7D_{3/2}) = 6$ MHz. This value is not a limit on the size of $B(7D_{3/2})$; we provide it to illustrate the sensitivity of $A(7D_{3/2})$ to $B(7D_{3/2})$. Again for illustrative purposes only, if we assume that $B(7D_{3/2}) = 64$ MHz [as large as $B(7D_{5/2})$] then we obtain $A(7D_{3/2}) = 17$ MHz. Table II compares the hyperfine constants we obtain with those predicted in Refs. [26,27]. The calculations of Ref. [26] do not include contributions from structural radiation, which can be significant for the D states.

B. Energy

Using the known hyperfine splitting of the $7S_{1/2}$ ground state (46 768.2 ± 2.6 MHz) [20] and the wavelengths of the trap laser (13 923.381 cm^{-1}) and probe laser, as measured by the wavemeter, we ascertain the difference from the accessible $7D_J$ hyperfine states to the ground-state center of gravity. Table III lists these energies. We use the hyperfine constants to extrapolate the energies of the inaccessible hyperfine levels. As discussed above, we assume that $B(7D_{3/2})=0$. From the measured and extrapolated hyperfine splittings we determine the center-of-gravity energy difference to the ground state $E(7D_J)$. The largest error comes from the precision of the wavemeter measurement of the trap and probe laser wavelengths. The wavelengths are measured independently so we add the individual error (0.002 cm^{-1}) in quadrature to obtain 0.003 cm^{-1}. Additional error considerations include uncertainties due to the effects discussed in measuring the hyperfine splittings, uncertainties in the ground-state hyperfine structure (0.0001 cm^{-1}), and the statistical error (0.0003 cm^{-1}). Table IV compares our measured values with *ab initio* and semi-empirical predictions.

The lowest-lying members of the nD_J series, the $6D_J$ levels, have not yet been observed. We repeat the quantum-

TABLE IV. Comparison of measured and predicted center-of-gravity energy difference to ground state using measured and extrapolated hyperfine splittings and assuming $B(7D_{3/2})=0$. The *ab initio* many-body perturbation theory (MBPT) calculations of Ref. [28] include second-order correlations. Reference [3] includes higher-order correlations: screening of the electron-electron interactions, particle-hole interactions, and iterations of the self-energy operator. The calculations of Ref. [27] include single, double, and some triple excitations. Values in Ref. [29] and the last two rows of the table are obtained from semi-empirical quantum-defect fits (QDF). To compare each of the theoretical energies with the measured energy, the calculated removal energy of the $7D_J$ state is subtracted from the experimentally obtained ionization potential [13].

Source	$E(7D_{3/2})$ (cm^{-1})	$E(7D_{5/2})$ (cm^{-1})
This work	**24 244.831(4)**	**24 333.298(4)**
Ref. [28] (MBPT)	24 235(120)	24 325(120)
Ref. [3] (MBPT)	24186	24275
Ref. [27] (MBPT)	24253	24343
Ref. [29] (second order QDF)	24 244.03(3)	24 332.93(3)
Second-order QDF, using δ from [13]	24 244.070	24 332.766
Third-order QDF, using $E(nD_J)$ from [13]	24 244.303	24 334.211

TABLE V. Comparison of measured and predicted values for the 7D fine-structure interval. See the caption of Table IV for a brief description of the different predictions. The last row is the result of a third-order quantum-defect fit using Eq. (3) and the center-of-gravity energies from Ref. [13].

Source	$\Delta E_{fine}(7D)$ (cm^{-1})
This work	**88.467(4)**
Ref. [28] (MBPT)	90
Ref. [3] (MBPT)	89
Ref. [27] (MBPT)	90
Ref. [29] (second-order QDF)	88.90
Second-order QDF, using δ from [13]	88.696
Third-order QDF, using $E(nD_J)$ from [13]	89.908
Third-order fine structure QDF	88.775

defect fits of the nD_J series including the $7D_J$ energies to calculate the energies of the $6D_J$ levels. Using the same approach in the S series guided us very well to the location of the 8S state [18,19]. The predicted center-of-gravity energy differences to the ground state are $16\,265\pm9$ cm^{-1} and $16\,453\pm9$ cm^{-1} for the $6D_{3/2}$ and $6D_{5/2}$ levels, respectively.

C. Fine structure

The fine-structure splitting of the 7D states is 88.467 ± 0.004 cm^{-1}. This lies within one percent of the *ab initio* prediction of 89 cm^{-1} by Dzuba *et al.* [3] and within 1.5% of the calculations of Safronova and Johnson [27]. Table V compares the measured fine structure with calculated values [3,27–29]. In the D states of all other alkalis except Li the fine structure is inverted [30]. Although this trend is reversed here, the mechanism that causes this inversion in the other alkalis and also causes the inverted hyperfine structure of the $nD_{5/2}$ states, namely, electron correlations, is the dominant contribution to the fine-structure splitting of the 7D states in Fr [31]. In one model of these correlations, the largest contribution arises when the valence d electron attracts a core electron such as a 6p or 6s electron with spin parallel to the 7d electron. (Inner-shell p and s electrons also participate to a lesser degree.) This leaves a net density of core electrons near the nucleus with opposite spin. Their spin-orbit and dipole hyperfine interactions are opposite in sign relative to the valence electron. If the magnitude of this indirect contribution is larger than the direct contribution from the 7d electron, it can invert the sign of the interaction. An equivalent model relies on configuration mixing between the 7D states and D states created by double excitation of the valence electron to a d state and a core 6p electron to the 7p state.

VI. CONCLUSION

We have used optical double-resonance spectroscopy on a cold sample of trapped Fr atoms to find the location of the 7D states. We extract fine and hyperfine splittings from our spectroscopic studies.

These new measurements of the D levels invite new calculations of francium's atomic and nuclear structure. They are particularly important since these levels present an interesting alternative for a parity nonconservation measurement [32]. They have a completely different series of systematic problems compared to those of the first excited S state [33].

ACKNOWLEDGMENTS

This work has been supported by the NSF. We thank C. T. Langlois for contributing to these measurements. We also thank V. A. Dzuba, V. V. Flambaum, M. S. Safronova, and W. R. Johnson for helpful discussions and for sharing with us preliminary unpublished results.

APPENDIX: AUTLER-TOWNES SPLITTING AND THE TRAP DETUNING

Because Fr has no stable isotopes, there is no reference transition with which to lock the trap laser. Instead, the trap laser is tuned to maximize fluorescence from the trap and

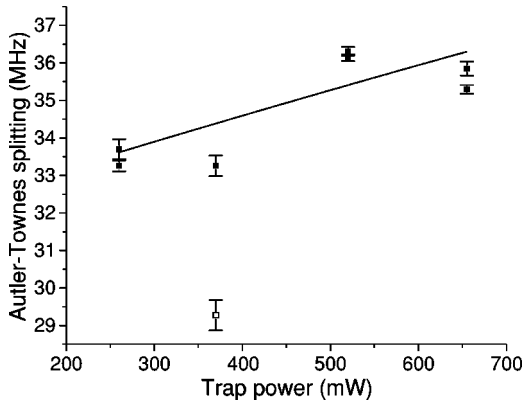

FIG. 7. Autler-Townes splitting of the transitions to the $7D_{3/2}$, $F=15/2,13/2$ levels plotted vs. total trap laser power. The curve is the best fit to Eq. (A2), yielding $\delta_{\rm trap}=-31.7\pm1.8$ MHz and $\Omega_{\rm trap}=\sqrt{CP_{\rm trap}}=15.8\pm3.4$ MHz for the normal trap operating conditions of 520 mW and a detuning that maximizes the trap fluorescence. The hollow data point is the result of measurements taken after the trap optics were realigned, so the constant of proportionality C may be different. The signal-to-noise ratio for the measurements was also much worse than for the other data. The point was included in the fit, however. Omitting it does not change the fit significantly: $\delta=-32.2\pm1.5$ MHz and $\Omega_{\rm trap}=12.6\pm3.8$ MHz.

then locked using a computer-controlled scanning Fabry-Perot cavity. The presence of the Autler-Townes splittings appearing in two-photon excitation of the $7D$ levels allows us to determine δ_{trap}. From Eq. (4), the Autler-Townes splittings Ω' should be given by

$$\Omega' = \sqrt{\Omega_{\mathrm{trap}}^2 + \delta_{\mathrm{trap}}^2}. \tag{A1}$$

The Rabi frequency Ω_{trap} is proportional to the amplitude of the electric field of the laser. Thus, Ω_{trap}^2 is proportional to the trap laser power P_{trap} through a constant C. Fitting the measured Autler-Townes splittings at different trap laser powers to

$$\Omega' = \sqrt{CP_{\mathrm{trap}} + \delta_{\mathrm{trap}}^2} \tag{A2}$$

gives $\delta_{\mathrm{trap}} = -31.7 \pm 1.8$ MHz and $\Omega_{\mathrm{trap}} = \sqrt{CP_{\mathrm{trap}}} = 15.8 \pm 3.4$ MHz for the normal trap operating conditions of 520 mW (See Fig. 7). Fitting the Autler-Townes splittings at different trap detunings to Eq. (A1) with Ω_{trap} fixed at 15.8 MHz gives $\delta_{\mathrm{trap}} = -30.9 \pm 0.9$ MHz at normal trap operating conditions. Combining the results yields $\delta_{\mathrm{trap}} = -31.1 \pm 0.6$ MHz. To test the validity of the results, we independently determine Ω_{trap}. We measure the intensity profile of the trapping beams and calculate the average intensity over the volume of the trap. Using a saturation intensity $I_{\mathrm{sat}}(7S_{1/2} \rightarrow 7P_{3/2}) = 7$ mW/cm^2 [34], we find $\Omega_{\mathrm{trap}} = 16.2$ MHz, confirming the fits.

[1] J. E. Simsarian, L. A. Orozco, G. D. Sprouse, and W. Z. Zhao, Phys. Rev. A **57**, 2448 (1998).

[2] J. S. Grossman, L. A. Orozco, M. R. Pearson, J. E. Simsarian, G. D. Sprouse, and W. Z. Zhao, Phys. Rev. Lett. **83**, 935 (1999).

[3] V. A. Dzuba, V. V. Flambaum, and O. P. Sushkov, Phys. Rev. A **51**, 3454 (1995).

[4] M. S. Safronova, W. R. Johnson, and A. Derevianko, Phys. Rev. A **60**, 4476 (1999).

[5] J. E. Simsarian, S. Aubin, J. S. Grossman, L. A. Orozco, M. R. Pearson, G. D. Sprouse, and W. Z. Zhao, in *Parity Violations in Atoms and Polarized Electron Scattering*, edited by Bernard Frois and Marie-Anne Bouchiat (World Scientific, Singapore, 1999), p. 312.

[6] W. Demtröder, *Laser Spectroscopy* (Springer-Verlag, New York, 1996).

[7] H. J. Metcalf and P. v. der Straten, *Laser Cooling and Trapping* (Springer-Verlag, New York, 1999).

[8] R. W. Fox, S. L. Gilbert, L. Holberg, J. H. Marquadt, and H. G. Robinson, Opt. Lett. **18**, 1456 (1993).

[9] C. Fort, F. S. Cataliotti, P. Raspollini, G. M. Tino, and M. Inguscio, Z. Phys. D: At., Mol. Clusters **34**, 91 (1995).

[10] T. T. Grove, V. Sanchez-Villianca, B. C. Duncan, S. Maleki, and P. L. Gould, Phys. Scr. **52**, 271 (1995).

[11] N. Ph. Georgiades, E. S. Polzik, and H. J. Kimble, Opt. Lett. **19**, 1474 (1994).

[12] G. D. Sprouse and L. A. Orozco, Annu. Rev. Nucl. Part. Sci. **47**, 429 (1997).

[13] E. Arnold, W. Borchers, M. Carré, H. T. Duong, P. Juncar, J. Lermé, S. Liberman, W. Neu, R. Neugart, E. W. Otten, M. Pellarin, A. Pesnelle, J. Pinard, J. L. Vialle, K. Wendt, and the ISOLDE Collaboration, J. Phys. B **22**, L391 (1989); E. Arnold, W. Borchers, H. T. Duong, P. Juncar, J. Lermé, P. Lievans, W. Neu, R. Neugart, M. Pellarin, J. Pinard, J. L. Vialle, K. Wendt, and the ISOLDE Collaboration, *ibid.* **23**, 3511 (1990).

[14] J. E. Simsarian, A. Ghosh, G. Gwinner, L. A. Orozco, G. D. Sprouse, and P. A. Voytas, Phys. Rev. Lett. **76**, 3522 (1996).

[15] W. Z. Zhao, J. E. Simsarian, L. A. Orozco, W. Shi, and G. D. Sprouse, Phys. Rev. Lett. **78**, 4169 (1997).

[16] W. Z. Zhao, J. E. Simsarian, L. A. Orozco, and G. D. Sprouse, Rev. Sci. Instrum. **69**, 3737 (1998).

[17] J. Ye, S. Swartz, P. Jungner, and J. L. Hall, Opt. Lett. **21**, 1280 (1996); G. P. Barwood, P. Gill, and W. R. C. Rowley, Appl. Phys. B: Photophys. Laser Chem. **53**, 142 (1991).

[18] J. E. Simsarian, W. Z. Zhao, L. A. Orozco, and G. D. Sprouse, Phys. Rev. A **59**, 195 (1999).

[19] J. E. Simsarian, W. Shi, L. A. Orozco, G. D. Sprouse, and W. Z. Zhao, Opt. Lett. **21**, 1939 (1996).

[20] A. Coc, C. Thibault, F. Touchard, H. T. Duong, P. Juncar, S. Liberman, J. Pinard, J. Lermé, J. L. Vialle, S. Büttgenbach, A. C. Mueller, A. Pesnelle, and the ISOLDE Collaboration, Phys. Lett. **163B**, 66 (1985).

[21] K. B. MacAdam and W. H. Wing, Phys. Rev. A **13**, 2163 (1976); C. Fabre, M. Gross, and S. Haroche, Opt. Commun. **13**, 393 (1975); K. C. Harvey and B. P. Stoicheff, Phys. Rev. Lett. **38**, 537 (1977).

[22] C. Delsart and J.-C. Keller, J. Phys. (Paris) **39**, 350 (1978).

[23] J. H. Marquadt, H. G. Robinson, and L. Hollberg, J. Opt. Soc. Am. B **13**, 1384 (1996).

[24] R. M. Whitley and C. R. Stroud, Jr., Phys. Rev. A **14**, 1498 (1976).

[25] T. P. Dinneen, C. D. Wallace, K.-Y. N. Tan, and P. L. Gould, Opt. Lett. **17**, 1706 (1992).

[26] V. A. Dzuba and V. V. Flambaum (private communication). Dzuba and Flambaum calculated hyperfine constants for ^{211}Fr. To compare with our measurements in ^{210}Fr, we scale these values using $AI/\mu_I = A'I'/\mu_I'$ and the values of the isotopes' nuclear magnetic moment from C. Ekström, L. Robertsson, and A. Rosén, Phys. Scr. **34**, 624 (1986).

[27] M. S. Safronova and W. R. Johnson (private communication).

[28] V. A. Dzuba, V. V. Flambaum, and O. P. Sushkov, Phys. Lett. **95A**, 230 (1983).

[29] E. Biémont, P. Quinet, and V. Van Renterghem, J. Phys. B **31**, 5301 (1998).

[30] C. E. Moore, *Atomic Energy Levels*, Natl. Bur. Stand. (U.S.) Circ. No. 467 (U.S. GPO, Washington D.C., 1958).

[31] V. A. Dzuba (private communication); V. V. Flambaum (private communication).
[32] N. Fortson, Phys. Rev. Lett. **70**, 2383 (1993).
[33] C. S. Wood, S. C. Bennett, J. L. Roberts, D. Cho, and C. E. Wieman, Can. J. Phys. **77**, 7 (1999).
[34] $I_{sat}(7S_{1/2}\rightarrow 7P_{3/2})=7$ mW/cm^2, scaling the two-level saturation intensity of 2.7 mW/cm^2 to account for the magnetic sublevels as described by Ref. [25].